Determination of the Three-Dimensional Structure of Iberiotoxin in Solution by ^1H Nuclear Magnetic Resonance Spectroscopy

Bruce A. Johnson*,‡ and Elizabeth E. Sugg§,‖

Departments of Biophysical Chemistry and Exploratory Chemistry, Merck Research Laboratories, P.O. Box 2000, Rahway, New Jersey 07065

Received March 17, 1992; Revised Manuscript Received June 2, 1992

ABSTRACT: The solution structure of chemically synthesized iberiotoxin, a scorpion toxin that blocks Ca^{2+}-activated K^+ channels, has been determined using 2D ^1H NMR spectroscopy. Analysis of the NOEs, coupling constants, and HN–DN exchange rates indicates the structure consists of an antiparallel β-sheet from residues 25 to 36, with a type 1 turn at residues 30–31, and a helix from residues 13 to 21. The carboxyl-terminal residues form a short, and distorted, third strand of the sheet. The NMR data are consistent with disulfide bonds from residues 7 to 28, 13 to 33, and 17 to 35. The disulfide bridging presents the same profile as in other scorpion toxins, where a Cys-X-Cys sequence in a strand of sheet forms two disulfide bonds to a Cys-X-X-X-Cys sequence in a helix. Three-dimensional structures were generated using the torsion angle space program PEGASUS. The best ten structures had an average rmsd over all pairwise comparisons of 1.49 Å. The average rmsd to a calculated average structure is 1.0 Å. The resulting structures appear very similar to those of charybdotoxin, a related scorpion toxin.

Peptidyl toxins that are found in venoms often function by interacting with and modulating the activity of ion channels. These toxins provide a means to probe the activities of different ion channels and obtain information on their physiological roles (Garcia et al., 1991). Two related toxins that have proved useful for probing the activity of calcium-activated potassium (BK or maxi-K) channels have been isolated from the venom of scorpions. Charybdotoxin, isolated from *Leiurus quinquestriatus hebraeus* (Miller et al., 1985), and iberiotoxin, isolated from *Buthus tamulus* (Galvez et al., 1990), are small globular polypeptides of 37 amino acids. The amino acid sequences of these two toxins are 68% identical (Figure 1) (Gimenez-Gallego et al., 1988; Sugg et al., 1990).

Both of these peptides are potent inhibitors of maxi-K channels when added to the extracellular side. Addition of the ChTX[1] to channels results in silent periods interspersed with normal channel activity (Miller et al., 1985). ChTX acts by reversibly blocking channel currents, without affecting channel gating (Anderson et al., 1988). Internal K^+ destabilizes the ChTX–channel interaction in a manner consistent with binding of K^+ to a site within the channel pore (MacKinnon & Miller, 1988). The fact that ChTX is competitive with TEA suggests that it interacts with the channel mouth near the pore (Miller, 1988). Recent studies by Giangiacomo et al. (1992) demonstrate that these essential properties of the ChTX–channel interaction are conserved in the IbTX–channel interaction. That is, IbTX binding also results in silent periods interspersed with normal channel activity, reversibly blocks channel currents without affecting channel gating, is competitive with TEA, and is destabilized by internal K^+. Thus it is likely that IbTX binds in a manner similar to that proposed for ChTX.

```
ChTX  pQFTNVSCTTSKECWSVCQRLHNTSRGKCMNKKCRCYS
IbTX  pQFTDVDCSVSKECWSVCKDLFGVDRGKCMGKKCRCYQ
```

FIGURE 1: Amino acid sequences of IbTX and ChTX. Identical residues are boxed. The first residue, pQ, is pyroglutamine.

Despite these fundamental similarities in the channel modulation properties of IbTX and ChTX, there are quantitative differences in their interactions with these channels (Giangiacomo et al., 1992). In particular, IbTX binding to the channel leads to significantly longer periods of channel blockage. The k_{off} value for iberiotoxin is approximately 10-fold lower than that of charybdotoxin. The association rate of IbTX is approximately 5-fold slower than that for ChTX. Furthermore, whereas ChTX inhibits a variety of K^+ channels in addition to maxi-K channels, including both Ca^{2+}- and voltage-dependent channels, IbTX has thus far been shown to be uniquely selective for maxi-K channels (Garcia et al., 1991).

The functional differences of these related toxins provide an opportunity to probe the structural features of the toxins that modulate their individual interactions with maxi-K channels. The two peptides share six cysteines and six positively charged residues in sequentially conserved positions. The most striking sequence difference between charybdotoxin and iberiotoxin is the presence of four additional negatively charged amino acids in iberiotoxin. These amino acid differences suggest that IbTX is a much less basic peptide with a net charge +1 (assuming that Lys, Arg, Asp, and Glu residues are fully ionized) than charybdotoxin with a net charge +5. This charge difference may be particularly important in view of the hypothesis that negatively charged residues around the channel pore play a significant role in charybdotoxin binding (MacKinnon & Miller, 1989). Analysis of experimental data from channels functionally modified with the carboxyl group modifying reagent trimethyloxonium suggests that surface electrostatics play an important role in charybdotoxin binding to the maxi-K channel (MacKinnon & Miller, 1989; MacKinnon et al., 1989).

A detailed understanding of the interactions of these toxins with the channels can only be made, however, with knowledge

* To whom correspondence should be addressed.
‡ Department of Biophysical Chemistry.
§ Department of Exploratory Chemistry.
‖ Present address: Glaxo Inc., Research Triangle Park, NC 27709.

[1] Abbreviations: ChTX, charybdotoxin; DQF-COSY, double-quantum-filtered correlation spectroscopy; FFT, fast Fourier transform; IbTX, iberiotoxin; NMR, nuclear magnetic resonance; NOE, nuclear Overhauser effect; NOESY, 2D NOE spectroscopy; rmsd, root mean square deviation; TOCSY, total correlation spectroscopy; 2D, two dimensional.

0006-2960/92/0431-8151$03.00/0 © 1992 American Chemical Society

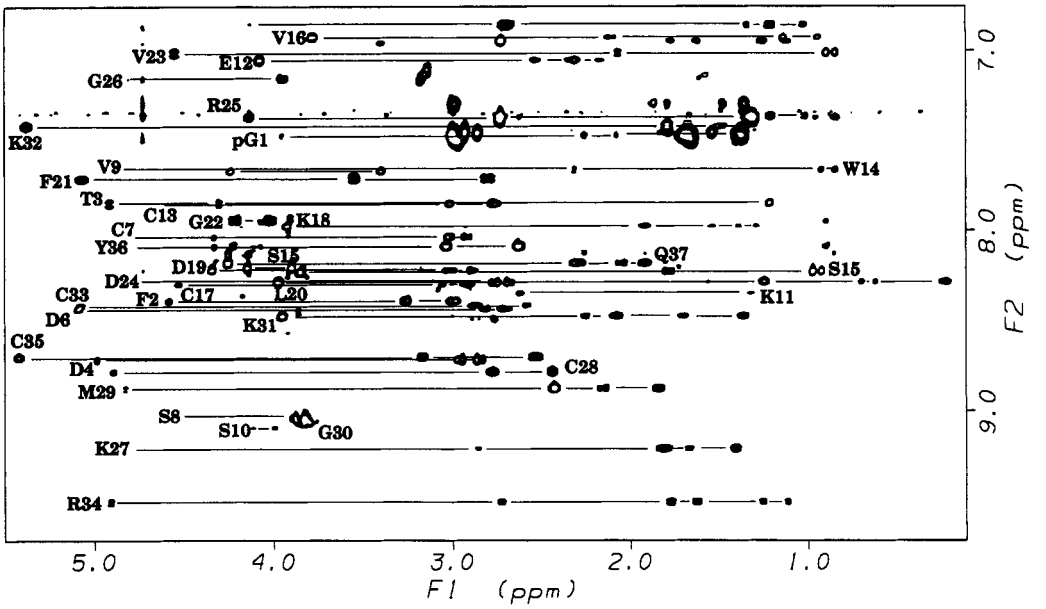

FIGURE 2: Contour plot of a TOCSY spectrum of iberiotoxin recorded with a spin lock period of 80 ms. Spin systems are labeled with the sequential residue position and with a line connecting the $C^{\alpha}H$ positions with the side-chain protons. Some cross-peaks for $C^{\alpha}H$ protons, though labeled, are not visible in this plot. These were observed at lower contour levels or in other spectra.

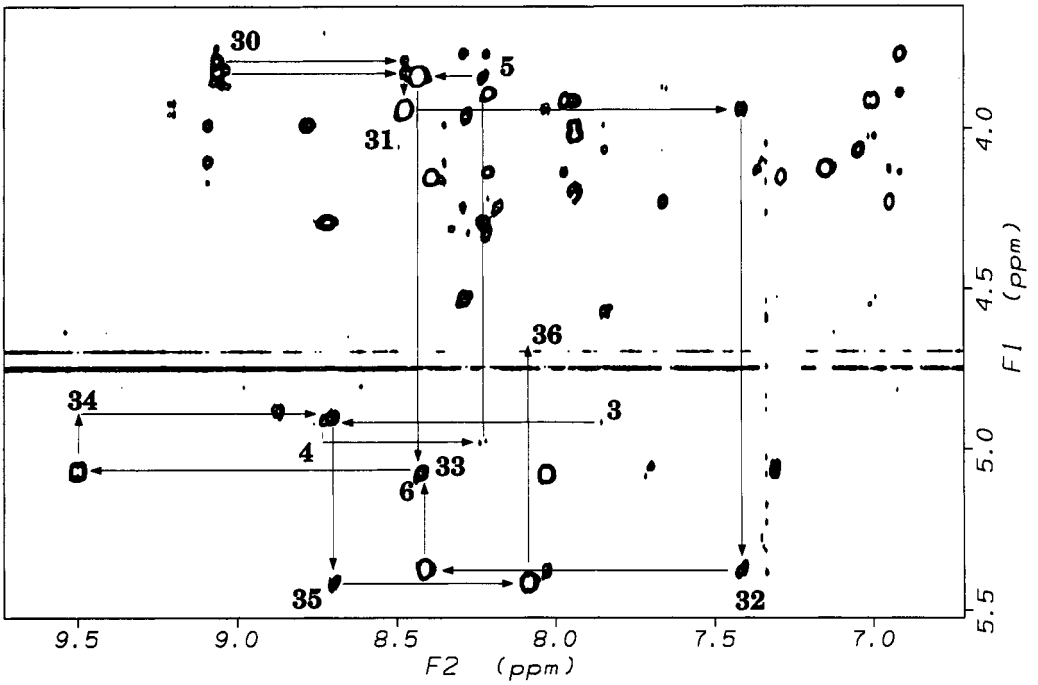

FIGURE 3: Contour plot of the fingerprint region of a NOESY spectrum of iberiotoxin recorded with 200-ms mixing time. The sequential $d_{\alpha N}$ connectivities for residues 3–6 and 30–36 are illustrated. Some cross-peaks for intraresidue HN–$C^{\alpha}H$ NOEs, though labeled, are not visible in this plot. These were observed at lower contour levels or in other spectra.

of the 3D structure of the toxins, such that the spatial position of conserved and differing residues is known. We describe in this paper the determination of the three-dimensional solution structure of iberiotoxin by the use of NMR spectroscopy. The resulting structure is very similar to the recently reported structure of charybdotoxin (Bontems et al., 1991a,b; Lambert et al., 1990), as opposed to the previously published charybdotoxin structure (since retracted) (Massefski et al., 1990, 1991).

MATERIALS AND METHODS

Sample Preparation. The iberiotoxin used was synthesized according to the protocol previously described for charybdotoxin (Sugg et al., 1990). A single sample of iberiotoxin was used for all NMR measurements. Four milligrams of iberiotoxin was dissolved in 550 μL of 90% H_2O/10% D_2O, for a final concentration of 1.7 mM. The pH of the sample was 3.2. A set of spectra were acquired under these conditions, and then the sample was lyophilized and redissolved in D_2O. All spectra were acquired at 25 °C. A limited set of experiments were performed at a higher pH (6.0) due to reduced solubility of the sample at this pH.

NMR Spectroscopy. All NMR measurements were performed on a Varian VXR 500 spectrometer using hypercomplex data acquisition (States et al., 1982). Identification of spin systems was obtained by analysis and comparison of two-dimensional DQF-COSY (Rance et al., 1983), TOCSY (Braunschweiler & Ernst, 1983; Davis & Bax, 1985), and

NOESY (Jeener et al., 1979; Macura et al., 1981) spectra. TOCSY spectra were acquired using MLEV-16 and a variety of mixing times ranging up to 80 ms (Bax & Davis, 1985). NOESY spectra were acquired in H_2O with mixing times of 50, 100, and 200 ms and in D_2O with mixing times of 80, 160, and 250 ms. Presaturation was used to suppress the water in all but two experiments. For two NOESY experiments water suppression was obtained by replacing the final 90° pulse with the jump–return sequence (90_x–τ–90_{-x}) (Plateau & Gueron, 1982). Processing and analysis of the spectra were done using the Varian VNMR software and FELIX (Hare Research Inc.).

Spectral Analysis. The positions of peaks in TOCSY and NOESY spectra were determined with a computer-facilitated procedure using the Varian MAGICAL software. A MAGICAL macro was written such that a single click of a menu button with the mouse would write the position of the cursor (in ppm) to a file. Using this macro the approximate positions of every peak in the spectra were quickly entered on a large-scale expansion of the spectra. A second pair of macros would then read sequentially through the above file, draw a small-scale expansion around the peak, allow the user to adjust the position of a bounding box around the peak, and write the new, precisely determined positions of the peak to a new file. With this methodology precise peak positions can be recorded with speed and accuracy.

Analysis of the spin coupling constant, $^3J_{HN\alpha}$, was done by analysis of absorptive and dispersive rows of the DQF-COSY spectrum (Kim & Prestegard, 1989). The position of a row (parallel to F_2) of the 2D FFT processed data matrix on each side of the center of every resolved NH–C$^\alpha$H cross-peak was determined. Each row was read in (using FELIX), and the splitting between the maxima of the absorption phase peak was determined. Then a Hilbert transform was performed to regenerate the complex data and a 90° zero-order phase shift was applied to generate the dispersive data. The splitting between the maxima of the dispersive peaks was determined. The coupling constants were then calculated as described (Kim & Prestegard, 1989). The two values from each side of the cross-peak were averaged.

Hydrogen–Deuterium Exchange. The rate of exchange of amide protons with solvent deuterons was determined qualitatively by following the disappearance of amide proton peaks from 1D spectra and 2D NOESY spectra. A sample lyophilized from 90% H_2O was dissolved in D_2O and immediately placed into the NMR spectrometer. The first spectrum was acquired within 4 min of the dissolution of the sample. One-dimensional spectra were acquired every 5 min over the first hour after dissolution. Then, 2D NOESY spectra, each taking approximately 5 h, were acquired at 90 min, 6 h, and 12 h after dissolution. These 2D spectra, which contained cross-peaks from only those amide protons that were slow to exchange with solvent, were useful for confirming sequential assignments.

Structure Determination. The determination of structures consistent with the experimental data was done using the program PEGASUS. PEGASUS is a program integrating molecular graphics, structure determination, and structure analysis. A detailed description of PEGASUS will be presented elsewhere (Johnson, in preparation). Here, a brief summary of its salient features is given.

The structure determination algorithm in PEGASUS is based on the variable target function method (Braun & Go, 1985). Structure refinement occurs in dihedral angle space using a rigid geometry model for the 20 amino acids (Robson & Platt, 1986). The refinement method involves a user-selected mix of conjugate gradient minimization (Press, 1991) using derivatives calculated with recurrent equations (Abe et al., 1984) and a simulated annealing protocol based on the Metropolis algorithm (Press, 1991). Use of the Metropolis algorithm provides a method, in contrast to the conjugate gradient technique, which can allow the structure to escape from local minima. Additionally, the dihedral angle changes at each step are bounded by user-controlled parameters. In contrast, the conjugate gradient minimizer can make very large changes in dihedral angles when large violations of the target function are present, thus causing large distortions of the structure. By use of the Metropolis algorithm after each introduction of additional constraints, the large violations are gently eliminated without gross distortion of the structure.

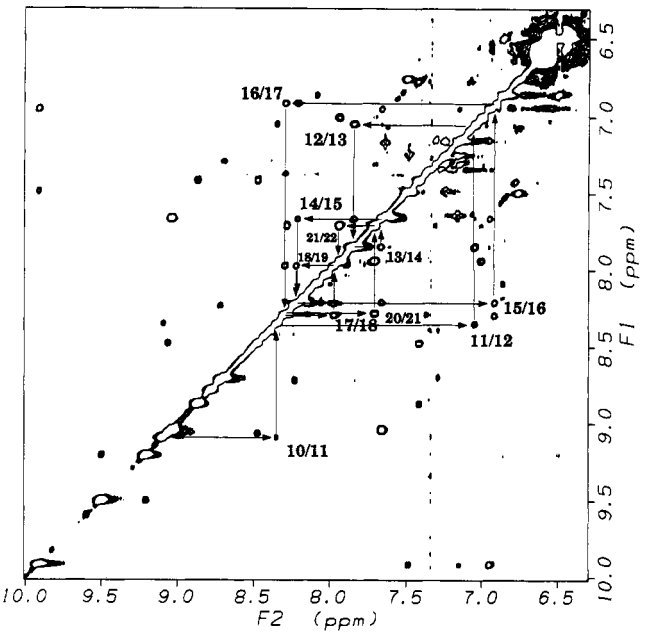

FIGURE 4: Contour plot of the amide proton region of a NOESY spectrum of iberiotoxin recorded with 200-ms mixing time. The sequential d_{NN} connectivities for residues 10–22 are illustrated.

The target function is a combination of the terms:

$$E_{total} = E_{NB} + E_{NOE} + E_{\phi} + E_{hbond} + E_{disulfide}$$

E_{NB} simulates the energy of contact between nonbonded atoms and is user selectable between a simple rapid potential function (Nilges et al., 1988) and a more complex but slower potential function (Robson & Platt, 1986). E_{NOE} is a potential which has the desirable property of remaining finite at large distance violations (Nilges et al., 1988). Pseudoatoms are used where diastereotopic protons cannot be distinguished from each other. PEGASUS automatically adds an appropriate distance to upper bounds involving pseudoatoms (Wüthrich, 1986). E_ϕ is a square well dihedral angle potential term used to constrain the backbone torsion angles to values consistent with $^3J_{HN\alpha}$ data. $E_{disulfide}$ is used to provide constraints between atoms in disulfide bonds and E_{hbond} to provide constraints between atoms in hydrogen bonds. The same potential form is used for $E_{disulfide}$ and E_{hbond} as in E_{NOE}, again so that the potential due to large violations is not excessive. The S(i)–S(j) distance is constrained to 2.0 Å, and the C$^\beta$(i)–S(j) and S(i)–C$^\beta$(j) distances are constrained to 3.0 Å for a disulfide bond between residues i and j. The HN(i)–O(j) distance is constrained to 1.9 Å, and the N(i)–O(j) distance is constrained to 2.9 Å for a hydrogen bond between residues i and j.

The variable target method (Braun & Go, 1985) is used in the sense that only energy terms between residues less than

Table I: Chemical Shifts (ppm) of Iberiotoxin in 90% H_2O at pH 3.3

residue	NH	$C^{\alpha}H$	$C^{\beta}H$	others
pE 1	7.30	4.15	1.88/1.80	H^{γ} 1.37
F 2	8.40	4.60	3.27/3.01	H^{δ} 7.27, H^{ϵ} 7.34
T 3	7.85	4.92	4.31	H^{γ} 1.23
D 4	8.72	5.00	2.97/2.87	
V 5	8.23	3.86	1.80	H^{γ} 0.99/0.94
D 6	8.44	5.08	2.82/2.72	
C 7	8.04	4.55	3.02/2.93	
S 8	9.05	4.64	3.90/3.84	
V 9	7.67	4.79	2.32	H^{γ} 0.94/0.87
S 10	9.10	4.13	4.19/4.01	
K 11	8.37	2.62	1.34	H^{ϵ} 2.72, H^{ζ} 7.36
E 12	7.06	4.09	2.32/2.18	H^{γ} 2.55
C 13	7.85	4.64	3.02/2.77	
W 14	7.67	4.25	3.40	$H^{\delta 1}$ 7.00, $H^{\epsilon 3}$ 7.60, $H^{\zeta 3}$ 7.17, $H^{\eta 2}$ 7.25, $H^{\zeta 2}$ 7.49
S 15	8.21	4.16	3.91/3.84	
V 16	6.93	3.79	2.12	H^{γ} 1.15/0.96
C 17	8.30	4.54	3.06/2.93	
K 18	7.98	3.95	1.93/1.79	H^{γ} 1.40/1.31, H^{δ} 1.55, H^{ϵ} 2.93, H^{ζ} 7.45
D 19	8.23	4.35	3.02/2.91	
L 20	8.29	3.98	1.26/0.24	H^{γ} 1.58, H^{δ} 0.71/0.64
F 21	7.72	5.08	3.56/2.81	H^{δ} 7.32, H^{ϵ} 7.15, H^{ζ} 7.26
G 22	7.96	4.22/4.03		
V 23	7.02	4.56	2.08	H^{γ} 0.91/0.87
D 24	8.29	4.64	2.77/2.69	
R 25	7.38	4.15	1.36/1.23	H^{γ} 1.04, H^{δ} 2.71, H^{ϵ} 6.86
G 26	7.16	4.85/3.93		
K 27	9.21	4.81	1.82	H^{γ} 1.42, H^{δ} 1.68, H^{ϵ} 2.87, H^{ζ} 7.46
C 28	8.79	4.91	2.78/2.45	
M 29	8.88	4.83	2.17	H^{γ} 1.85, H^{ϵ} 2.44
G 30	9.06	3.86/3.79		
K 31	8.48	3.96	2.27/2.09	H^{γ} 1.38, H^{δ} 1.71, H^{ϵ} 3.01, H^{ζ} 7.48
K 32	7.43	5.39	1.80	H^{γ} 1.36, H^{δ} 1.48, H^{ϵ} 2.99, H^{ζ} 7.30
C 33	8.42	5.08	2.89/2.59	
R 34	9.51	4.92	1.79/1.64	H^{γ} 1.27/1.14, H^{δ} 2.74, H^{ϵ} 6.95
C 35	8.71	5.43	3.18/2.55	
Y 36	8.09	4.71	3.04/2.64	H^{δ} 6.90, H^{ϵ} 6.52
Q 37	8.19	4.26	2.30/2.06	H^{γ} 1.93

a certain window size are included at any stage of refinement. Two separate windows are used, one for the NOE term and one for all other interactions. The windows are incremented according to a user-specified schedule during the refinement process.

Upper and lower bound constraints were calculated from peak volumes in the NOESY spectra. Peak volumes were determined during the computer-facilitated assignment process described above. We examined buildup curves of every NOE cross-peak to eliminate the few cross-peaks that appeared to arise through spin diffusion. From the same buildup curves we could see that the deviation from linearity due to spin diffusion was minimal. The peak volumes were converted to approximate distance constraints. The lower bound for all constraints was 2 Å. The upper bound was calculated using the $1/r^6$ dependence of NOE intensity on distance (Wüthrich, 1986). The d_{NN} constraints were calibrated against the typical intensity of peaks in the helical region from residues 14 to 20, assuming a distance of 2.8 Å for d_{NN} (Wüthrich, 1986). All constraints between amide protons and non-amide protons were calibrated against the typical $d_{\alpha N}$ intensities in the β-sheet using a distance of 2.2 Å. All NOE intensities that did not involve amide protons were obtained from NOESY spectra in D_2O and were calibrated against the typical $d_{\alpha\alpha}$ intensity across the sheet, using a distance of 2.3 Å. To allow for molecular motion and imprecision in the calculated bounds, an extra 0.5 Å was added to all the upper bounds for NOE constraints involving backbone atoms and 0.7 Å to the upper bounds of NOE constraints involving side-chain atoms.

Constraints on the dihedral angle ϕ were obtained from the coupling constants $^3J_{HN\alpha}$. Dihedral angles where $^3J_{HN\alpha}$ ranged from 8 to 9 Hz were constrained to $-120° \pm 30°$, those from 9 to 10 Hz were constrained to $-120° \pm 20°$, and those above 10 Hz were constrained to $-120° \pm 15°$. Those below 6 Hz were constrained to $-70° \pm 30°$. Hydrogen-bonding constraints were explicitly used for those hydrogen bonds expected in the β-sheet which were all consistent with the observed pattern of HN–DN exchange rates and NOEs.

The structure determination proceeded as follows. Each starting structure was put into a random starting conformation such that the dihedral angles ϕ and ψ had random values within the extreme limits normally found in proteins (Ramachandran & Sasisekharan, 1963). Starting structures chosen in this manner have been suggested by Havel (1990). The nonbond window was set to a size of 2. This allows for the calculation of contacts within and between adjacent residues only. The constraint window was set to a size of 1, which allows for the inclusion of only intraresidue NOEs. Then 200 cycles of the Metropolis algorithm were executed, followed by 5 cycles of the conjugate gradient minimizer. The force constant on the experimental distance constraints was then increased to 100 kcal/(mol·Å), and 30 more cycles of conjugate gradient minimization were performed. The size of the nonbond and constraint windows was then incremented together according to the following schedule: 2, 3, 4, 5, 6, 7, 8, 9, 10, 15, 20, 25, 30, 35, 40. At each stage, the above sequence of the Metropolis algorithm and the conjugate gradient minimizer were executed.

After an initial set of structures was generated with a set of 130 unambiguous NOEs, the NOE identification facility of PEGASUS was used to identify additional NOEs. This facility is similar to that of the IDNOE program (Kline et al., 1990).

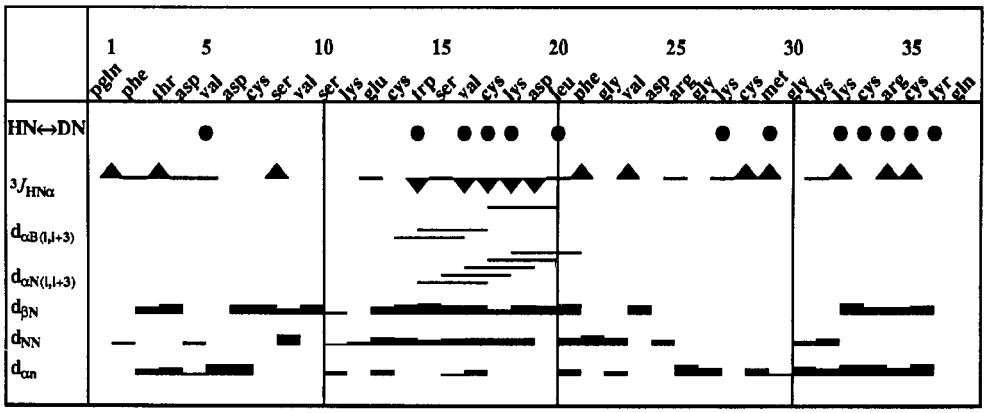

FIGURE 5: Summary of short-range NOEs ($|i-j| < 4$) involving NH, $C^{\alpha}H$, $C^{\beta}H$, $^3J_{HN\alpha}$, and amide proton exchange rates. The height of the lines for sequential NOEs is proportional to the upper distance bound calculated from the NOE intensity. Coupling constants, $^3J_{HN\alpha}$, greater than 8 Hz are indicated as (▲) and less than 6 Hz as (▼), and those with values between 6 and 8 Hz are indicated as (–). Amide protons persistent in the 1D spectra taken 90 min after exchange in D_2O are indicated as (●).

For each unassigned NOE, PEGASUS reports the set of possible atom pairs whose chemical shifts are within 0.02 ppm of the unknown cross-peak. For each atom pair it lists the shortest distance, the average distance, and the longest distance between those atoms in the set of preliminary structures. This information was checked against the actual spectra, and where a clear assignment based on the distance in the preliminary structures was possible, the NOE was added to the constraint list. An additional 18 distance constraints, for a total of 148, were extracted from the data. A second round of structure determination was then performed using the same protocol as above, also starting from randomized structures. The final set of NOEs consisted of 4 intraresidue, 86 sequential, 32 medium-range, and 26 long-range constraints.

Superposition, error analysis, and visual display of structures were done with PEGASUS. Calculation of dipole moments of the structures was done with the program Quanta (Polygen Corp.), version 3.2.3.

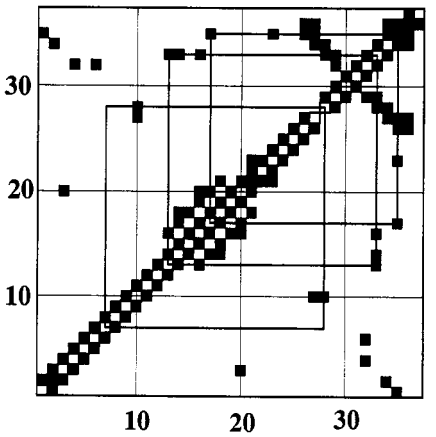

FIGURE 6: Summary of all NOE data. A filled square indicates that an NOE between some pair of atoms on the corresponding residues was observed. Heavy lines indicate the disulfide bond pairing that resulted from the analysis of the data, as described in the text.

RESULTS

Sequential Assignments. The sequence-specific assignment of resonances was performed using the now conventional procedures (Wüthrich, 1986). Cross-peaks between NH and $C^{\alpha}H$ protons were identified by examination of DQF-COSY spectra acquired in H_2O. TOCSY spectra with mixing times ranging up to 80 ms were used to correlate side-chain spin systems with the NH–$C^{\alpha}H$ cross-peaks (Figure 2). Ring protons of the Phe and Tyr residues were assigned by observation of NOEs to the β-protons. Intraresidue assignments were confirmed with DQF-COSY and TOCSY spectra in D_2O. These spin systems were then classified by virtue of their coupling pattern and chemical shifts into amino acid type or spin-system class.

NOESY cross-peaks of types $d_{\alpha N}$, d_{NN}, and $d_{\beta N}$ correlating sequentially adjacent amino acids were then used to assign spin systems to specific residues in the iberiotoxin sequence (Figures 3 and 4). The unique leucine, threonine, tyrosine, and tryptophan residues provided useful markers for the sequential assignments. The glycine, valine, phenyalanine, and serine residues, which were assignable to single amino acid type rather than to just spin-system class, were particularly useful in identifying stretches of sequentially adjacent residues. The only significant problem encountered in the assignment process involved several residues whose $C^{\alpha}H$ protons resonated close to the frequency of water. Two strategies were used to overcome this problem. First, NOESY spectra were acquired using a jump–return pulse for the final pulse so that the water (and underlying $C^{\alpha}H$ protons) was not saturated. Second, a NOESY spectrum was acquired over the 6-h period starting 90 min after transfer of the sample to D_2O. This spectrum required minimal water suppression, and connectivities involving the slowly exchanging NH protons in the sheet and helix were clearly observable. Using these methods the spin systems of all residues in the iberiotoxin sequence were assigned. The assigned resonances are listed in Table I.

Secondary Structure. The analysis of the secondary structure of iberiotoxin was based on the data summarized in Figures 5 and 6. As can be seen from Figure 5, the pattern of short- and medium-range NOEs, in particular d_{NN}, $d_{\alpha N(i,i+3)}$, and $d_{\alpha\beta(i,i+3)}$, seen for residues 13–21 is characteristic of that expected in a helix. This is confirmed by the small values of the $^3J_{HN\alpha}$ coupling and the slow rate of HN–DN exchange seen for the amide protons in this region. Since we did not definitively observe any $i,i+4$ NOEs, we are not prepared to classify this helix as an α-helix.

The pattern of NOEs seen in the region of residues 25–36 is consistent with that expected for an antiparallel β-sheet with a type 1 turn at residues G 30–K 31. In particular, the long-range $C^{\alpha}H(i)$–$C^{\alpha}H(j)$ NOEs are indicative of an antiparallel β-sheet structure. This is confirmed by the slow rate of exchange observed for all protons expected to be in hydrogen bonds in this sheet, as well as the large $^3J_{HN\alpha}$ values observed for most residues. With one exception, all $C^{\alpha}H$–$C^{\alpha}H$ and NH–$C^{\alpha}H$ NOEs expected in this β-sheet structure were observed. The single exception was due to chemical shift

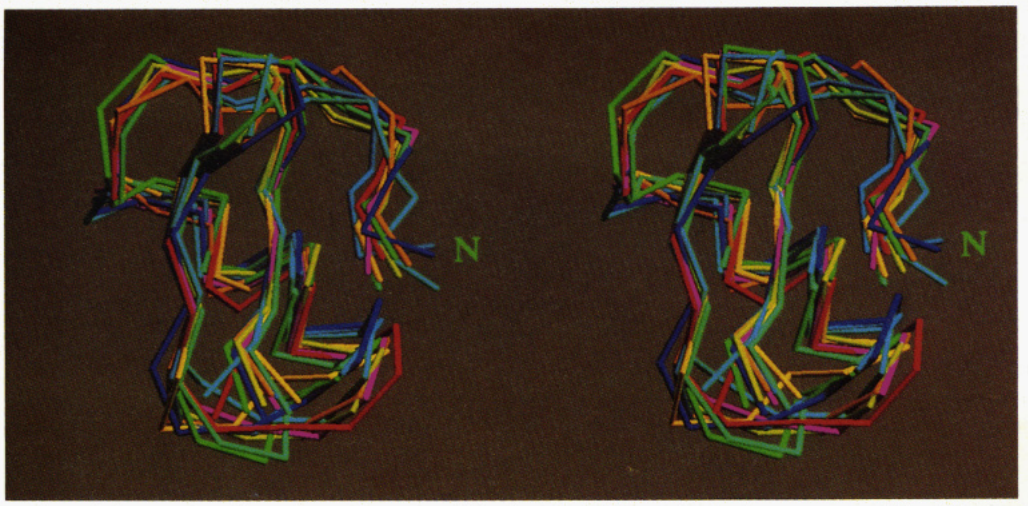

FIGURE 7: A stereoview of the superposition of ten structures of iberiotoxin as determined using PEGASUS. The C^{α} trace is shown and the amino terminus is labeled N.

degeneracy. A $C^{\alpha}H$–$C^{\alpha}H$ NOE between the C^{α} protons of residues 2 and 34 suggested a third strand of the sheet could be formed between 32–36 and 2–5. This is consistent with the slow NH exchange of some of the amide protons between these two strands. The absence of the expected strong NOE between C^{α} protons of residues 4 and 32, however, is inconsistent with the formation of a good sheet structure. This segment could be considered a third, but distorted, strand of the antiparallel B-sheet.

Disulfide Analysis. A crucial determinant of the tertiary structure of disulfide-linked proteins such as iberiotoxin or charybdotoxin is the elucidation of the connectivity pattern among the cysteine residues. With charybdotoxin we used enzymatic cleavage followed by amino acid analysis and peptide sequence analysis of the resulting fragments to identify the cysteine linkage profile (Sugg et al., 1990). These results were subsequently used by others in their protein structure determination of charybdotoxin using NMR spectroscopy (Bontems et al., 1991a). We tried the same approach with iberiotoxin but were unable to obtain good proteolytic cleavage and a clean separation of fragments. The very limited sample quantity precluded further attempts. Instead, we used analysis of the NMR data to assign the disulfides. As can be seen from Figure 6, two of the disulfides (13–33, 17–35) are suggested by NOEs between protons of the corresponding cysteine residues. We generated ten structures using the set of unambiguous NOE constraints without any disulfide constraints. The five best structures were analyzed using PEGASUS to determine the S^{γ}–S^{γ} distance for all possible pairings. The average S^{γ}–S^{γ} distance in the set of structures was lowest for the three disulfide pairs (7–28, 13–33, 17–35) that were found in the closely related peptide charybdotoxin (Sugg et al., 1990). These three pairs were used as the disulfide restraints for the structure determination.

Tertiary Structure. A total of 47 structures were calculated using the final set of 148 NOE constraints, 9 disulfide bond constraints, 5 hydrogen bond constraints, and 15 constraints on the dihedral angle ϕ. The ten structures having the lowest violations of the distance constraints were chosen for further analysis. Of these ten structures, there were two NOE constraint violations of 0.5 Å and two NOE constraint violations of 0.4 Å. All remaining violations were 0.3 Å or less. Figure 7 shows a superposition of the structures resulting from the PEGASUS analysis of the experimental NMR data. Residues 1–6 form an extended strand which turns and goes into the helix residues 12 to 20. A second turn through residues 21–24 leads into the antiparallel sheet from 25 to 36. A tight turn (type 1) is present in the sheet at residues 29–32. The helix is held in proximity to the sheet by two disulfides (13–33, 17–35). The third disulfide between residues 7–28 provides a connection between the initial extended strand and the rest of the structure. Figure 8 shows a space-filling model of the iberiotoxin structure.

The overall agreement among the different structures can be summarized by an rmsd value. Calculated as an average of rmsds of all pairwise combinations of the ten structures, the rmsd is 1.49 Å. The average of rmsds for pairwise combinations of all ten structures with a calculated average structure is 1.0 Å. As can be seen from the structures of Figure 7, the antiparallel sheet and the helix are well-defined. Significantly more variability is seen in the turn regions of residues 8–12, 21–24, and 30–31, as well as in the region of residues 10–12, and in the amino terminus from 1 to 7. This structural variability was quantified using an angular order parameter (Detlefsen et al., 1991). This parameter is formed for each dihedral angle by summing a vector representation of the corresponding angle in each structure and then dividing by the number of structures. The angular order parameter ranges from 0.0 to 1.0. A value of 1.0 is obtained if all the structures have the same value for a particular angle. The greater the dispersion of angles, the closer the order parameter is to 0.0. Figure 9 shows the angular order parameter for the backbone ϕ and ψ angles. Significant disorder is observed in the amino terminus and at the position of the two glycines (22 and 30) found in the turns. By this criterion, however, the helix and β-sheet are well ordered.

DISCUSSION

The three-dimensional structure of iberiotoxin is very similar to the recently published structures of charybdotoxin (Bontems et al., 1991a,b; Lambert et al., 1990). These two toxins share a motif consisting of a β-sheet connected to a helix by two pairs of disulfide-bridged cysteine residues. The disulfide bridging presents the same profile as in charybdotoxin, where a Cys-X-Cys sequence in a strand of sheet forms two disulfide bonds to a Cys-X-X-X-Cys sequence in the helix. As has been noted recently, this motif is present in all known scorpion toxins as well as in insect defensins (Bontems et al., 1991b).

The overall structural similarity of charybdotoxin and iberiotoxin is reflected in the striking similarity of chemical shifts observed between these two peptides. Figure 10

FIGURE 8: Two views of the space-filling model of the "best" iberiotoxin structure. The structure is colored according to the charge of the amino acid residues, with positive residues (Lys, Arg) in green, negative residues (Asp, Glu) in red, and neutral residues in white. The views differ by a 180° rotation about the y axis. Atoms are drawn at their van der Waals radius plus 1.4 Å.

illustrates the deviation from the random coil position for the H^{α} and HN chemical shifts. This chemical shift profile is reflective of the observed secondary structure. For example, the H^{α} shifts are all shifted upfield approximately 0.3 ppm in the helix and downfield approximately 0.5 ppm in the sheet. Recently, it was noted that amide proton chemical shifts in helices are periodic (Kuntz et al., 1991). While the helix is too short in IbTX or ChTX to observe a significant periodicity, the pattern of shifts observed is consistent with their observation. One of the most striking shifts apparent in Figure 10 is that of the H^{α} of Lys-11. This proton is shifted approximately 1.8 ppm upfield in both IbTX and ChTX, presumably a consequence of the proximity of the aromatic ring of Trp-14 which is brought close to 11 by virtue of the helix.

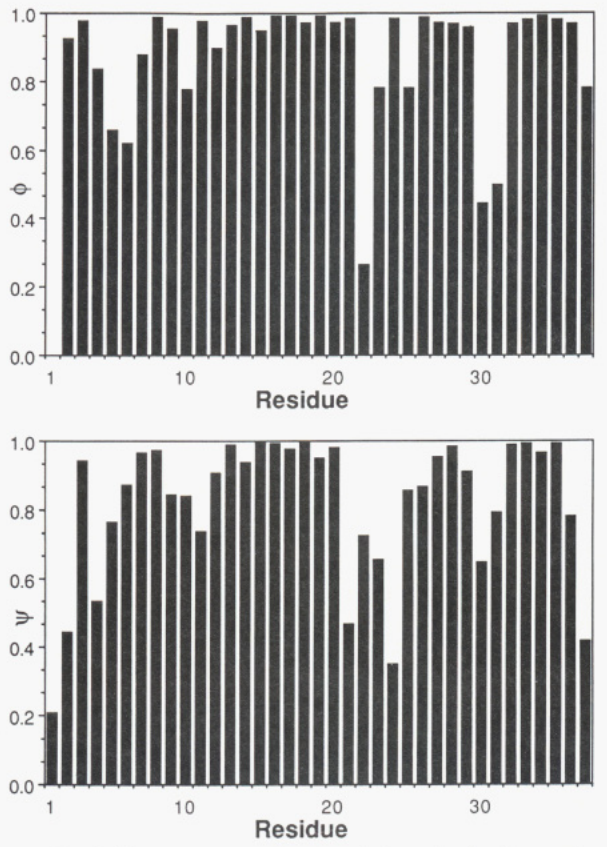

FIGURE 9: Order parameters for ϕ and ψ angles in the ten best structures. The closer the value is to 1.0, the more defined the angle is.

The differences in binding kinetics and channel specificity of the two toxins can be ascribed to at least three areas of differences between IbTX and ChTX. These are differences in net charge, electrostatic asymmetry, and specific residue–residue interactions between the toxins and the channel. First, the amino acid composition of the two toxins differs primarily in the presence of four additional negatively charged aspartate residues in IbTX. This results in a net charge of 5 on ChTX and 1 on IbTX (based on unit charges on each Asp, Glu, Lys, and Arg residue). This difference in charge on IbTX may account for its lower on-rate to the channel, as a result of reduced electrostatic attraction to the channel. If the negative charges on IbTX are also involved in binding, there may also be a larger energy cost involved in desolvating the additional charges on IbTX.

A second possible source of differences in binding kinetics between the toxins is differences in the electrostatic asymmetry of the two toxins. Presumably, toxin binding occurs in a specific orientation to the channel that results in blockage of the channel. Random diffusional interactions with the channel will result in many unproductive complexes that will reduce the apparent k_{on} below the diffusion-controlled factor. The facilitation of productive binding by orientation of reactants through electrostatic forces has previously been postulated to occur in protein–protein interactions. For example, Koppenol and Margoliash (1982) demonstrated that the reaction rate of various chemically modified cytochrome c molecules with three redox partners correlates with the dipole moment of the cytochrome c.

As described above, the interaction of toxin with the channel has been suggested to involve local electrostatic fields (MacKinnon & Miller, 1989; MacKinnon et al., 1989). Thus, the above mechanism of electrostatic steering could play a

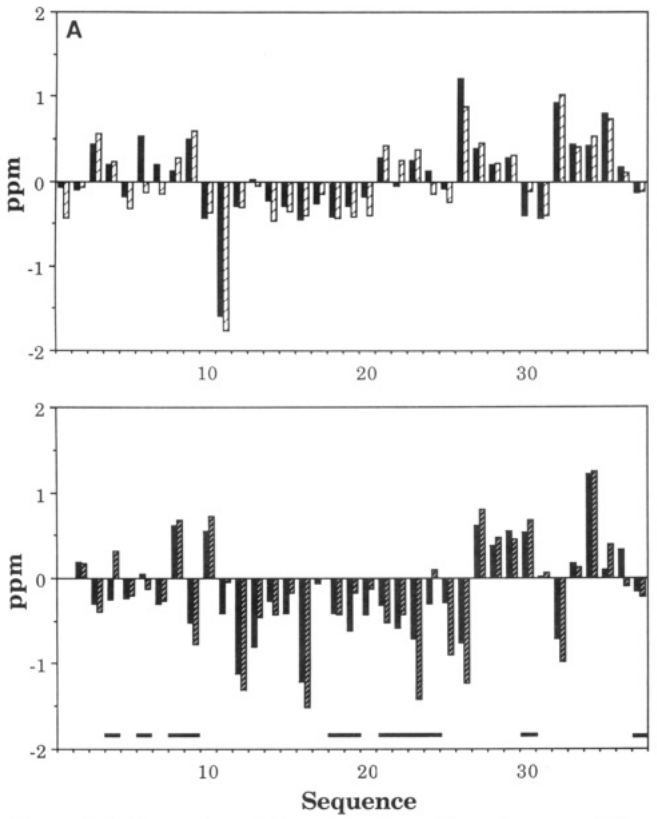

FIGURE 10: Comparison of the sequence-specific assignments of the chemical shifts of the C^{α}(A) and NH (B) protons of iberiotoxin and charybdotoxin. The chemical shifts are deviations from "random coil" values (Wüthrich, 1986). Horizontal bars indicate residues that differ between iberiotoxin and charybdotoxin.

role in the difference in binding of ChTX and IbTX to the maxi-K channel. A first-order approximation of the electrostatic asymmetry of these toxins can be obtained from a determination of their dipole moment. As we do not yet have the 3D coordinates of ChTX, we used the dihedral angles from the IbTX structure to generate a model with the ChTX sequence. IbTX has a significantly larger dipole moment (250 D) than that of our modeled ChTX structure (135 D), a result of the asymmetrical placement of the four additional aspartate residues. The dipole is oriented in a slightly different direction; the angle between that of IbTX and that of ChTX is 23°. If electrostatic steering plays a role in toxin binding, this difference in dipole moment could indeed be important. A more detailed comparison of the two toxins could be made with a calculation and graphical display of the electrostatic potentials and fields (Roberts et al., 1991).

Third, the largely conserved structure between ChTX and IbTX suggests that one may be able to ascribe the different interactions of IbTX and ChTX with the maxi-K channel to specific residues that differ between the two toxins. As discussed above, it has been hypothesized that negatively charged residues are present around the maxi-K channel pore and play an important role in ChTX binding (Massefski et al., 1991; Sugg et al., 1991; MacKinnon et al., 1989). In view of this, the disposition of the positively charged residues in IbTX and ChTX is particularly important. One striking feature is the presence of five of the seven Lys and Arg residues in the β-sheet. Their sequential positions in this sheet place their side chains all on one solvent-exposed face of the sheet. In consequence of this, the toxin presents a face which is largely positively charged. These residues all have conserved positions in IbTX and ChTX, and thus this face will be largely similar between the two toxins. In view of the postulated interaction of positively charged residues in the toxin with negatively charged residues on the channel, it is reasonable to conclude that this face of the toxin could be involved in the receptor interaction.

As can be seen in Figure 8, three of the additional negative residues (4, 6, and 19) are found on the opposite face from the positive charges. The fourth (24) is found on the edge between the two faces. The position of these residues is such that they leave the positively charged sheet face unaffected. It is possible that these negatively charged residues may form specific contacts with the channel upon binding that stabilize the toxin–channel interaction. This could be a source of additional binding energy that results in the significantly lower k_{off} value of IbTX from the channel.

A detailed understanding of the varied roles of these three views of toxin binding, net charge, electrostatic asymmetry, and specific residue–residue interactions, will now be feasible. The analysis of various modified toxins, either ChTX or IbTX in the light of our now detailed structural knowledge of ChTX (Bontems et al., 1991a) and IbTX (this paper), should allow us to understand the various mechanisms involved in toxin binding kinetics and specificity. An approach to this has been started with the construction of synthetic charybdotoxin–iberiotoxin chimeric peptides (Garcia et al., 1990). These peptides were, however, generated prior to our knowledge of the 3D structure of ChTX or IbTX. With our knowledge of the 3D structures it can now be seen that these sequence-based hybrids, formed from the amino and carboxyl halves of the two peptides, have simultaneous changes in residues at several places in the 3D structure. Hybrids and site-specific variants can now be constructed on the basis of our detailed understanding of the spatial position of the differing and conserved residues in the toxins.

ACKNOWLEDGMENT

We thank K. M. Giangiacomo, P. R. Gooley, O. B. McManus, and J. P. Springer for helpful discussions and critical suggestions on the manuscript and M. Garcia for assistance with sample purification.

REFERENCES

Anderson, C., MacKinnon, R., Smith, R., & Miller, C. (1988) *J. Gen. Physiol. 91*, 317–333.

Bax, A., & Davis, D. G. (1985) *J. Magn. Reson. 65*, 355–360.

Bontems, F., Roumestand, C., Boyot, P., Gilquin, B., Doljansky, Y., Ménez, A., & Toma, F. (1991a) *Eur. J. Biochem. 196*, 19–28.

Bontems, F., Roumestand, C., Gilquin, B., Ménez, A., & Toma, F. (1991b) *Science 254*, 1521–1523.

Braun, W., & Go, N. (1985) *J. Mol. Biol. 186*, 611–626.

Braunschweiler, L., & Ernst, R. R. (1983) *J. Magn. Reson. 53*, 521–558.

Davis, D. G., & Bax, A. (1985) *J. Am. Chem. Soc. 107*, 2820–2821.

Detlefsen, D. J., Thanabal, V., Pecoraro, V. L., & Wagner, G. (1991) *Biochemistry 30*, 9040–9046.

Galvez, A., Gimenez-Gallego, G., Reuben, J. P., Roy-Contancin, L., Feigenbaum, P., Kaczorowski, G. J., & Garcia, M. L. (1990) *J. Biol. Chem. 265*, 11083–11090.

Garcia, M. L., Sugg, E. E., Reuben, J. P., Patchett, A. A., & Kaczorowski, G. J. (1990) *Biophys. J. 57*, 118a.

Garcia, M. L., Galvez, A., Garcia-Calvo, M., King, V. F., Vazquez, J., & Kaczorowski, G. J. (1991) *J. Bioenerg. Biomembr. 23*, 615–646.

Giangiacomo, K. M., Garcia, M. L., & McManus, O. B. (1992) *Biochemistry* (in press).

Gimenez-Gallego, G., Navia, M. A., Reuben, J. P., Katz, G. M., Kaczorowski, G. J., & Garcia, M. L. (1988) *Proc. Natl. Acad. Sci. U.S.A. 85*, 3329–3333.
Havel, T. (1990) *Biopolymers 29*, 1565–1585.
Jeener, J., Meier, B. H., Bachman, P., & Ernst, R. R. (1979) *J. Chem. Phys. 71*, 4546–4553.
Kim, Y., & Prestegard, J. H. (1989) *J. Magn. Reson. 84*, 9–13.
Kline, T. P., Brown, F. K., Brown, S. C., Jeffs, P. W., Kopple, K. D., & Mueller, L. (1990) *Biochemistry 29*, 7805–7813.
Koppenol, W. H., & Margoliash, E. (1982) *J. Biol. Chem. 257*, 4426–4437.
Kuntz, I. D., Kosen, P. A., & Craig, E. C. (1991) *J. Am. Chem. Soc. 113*, 1406–1408.
Lambert, P., Kuroda, H., Chino, N., Watanabe, T. X., Kimura, T., & Sakakibara, S. (1990) *Biochem. Biophys. Res. Commun. 170*, 684–690.
MacKinnon, R., & Miller, C. (1988) *J. Gen. Physiol. 91*, 335–349.
MacKinnon, R., & Miller, C. (1989) *Biochemistry 28*, 8087–8092.
MacKinnon, R., Latorre, R., & Miller, C. (1989) *Biochemistry 28*, 8092–8099.
Macura, S., Huang, Y., Suter, D., & Ernst, R. R. (1981) *J. Magn. Reson. 43*, 259–281.
Massefski, W., Jr., Redfield, A. G., Hare, D. R., & Miller, C. (1990) *Science 249*, 521.
Massefski, W., Jr., Redfield, A. G., Hare, D. R., & Miller, C. (1991) *Science 252*, 631.
Miller, C. (1988) *Neuron 1*, 1003–1006.
Miller, C., Moczydlowski, E., Latorre, R., & Phillips, M. (1985) *Nature (London) 313*, 316–318.
Nilges, M., Clore, G. M., Gronenborn, A. M., & Brünger, A. T. (1988) *Protein Eng. 2*, 27–38.
Plateau, P., & Guéron, M. (1982) *J. Am. Chem. Soc. 104*, 7310–7311.
Press, W. (1991) *Numerical Recipes*, Cambridge University Press, New York.
Ramachandran, G. N., & Sasisekharan, V. (1963) *Adv. Protein Chem. 68*, 284–438.
Rance, M., Sørensen, O. W., Bodenhausen, G., Wagner, G., Ernst, R. R., & Wüthrich, K. (1983) *Biochem. Biophys. Res. Commun. 117*, 479–485.
Roberts, V. A., Freeman, H. C., Olson, A. J., Tainer, J. A., & Getzoff, E. D. (1991) *J. Biol. Chem. 266*, 13431–13441.
Robson, B., & Platt, E. (1986) *J. Mol. Biol. 188*, 259–281.
States, D. J., Haberkorn, R. A., & Ruben, D. J. (1982) *J. Magn. Reson. 48*, 286–292.
Sugg, E. E., Garcia, M. L., Reuben, J. P., Patchett, A. A., & Kaczorowski, G. J. (1990) *J. Biol. Chem. 265*, 18745–18748.
Wüthrich, K. (1986) *NMR of Proteins and Nucleic Acids*, John Wiley & Sons, New York.